HHS Public Access

Author manuscript

Neuroimage. Author manuscript; available in PMC 2015 March 14.

Published in final edited form as:

Neuroimage. 2013 July 1; 74: 266–275. doi:10.1016/j.neuroimage.2013.01.042.

Physiological and modeling evidence for focal transcranial electrical brain stimulation in humans: A basis for high-definition tDCS

Dylan Edwards[a,b,c,d,*], **Mar Cortes**[a,b], **Abhishek Datta**[e], **Preet Minhas**[e], **Eric M. Wassermann**[f], and **Marom Bikson**[e]

[a]Burke Medical Research Institute, White Plains, NY, USA

[b]Department of Neurology and Neuroscience, Weill Cornell Medical College, New York, NY, USA

[c]Berenson-Allen Center for Noninvasive Brain Stimulation, Beth Israel Deaconess Medical Center, Harvard Medical School, Boston, MA, USA

[d]Australian Neuromuscular Research Institute and the Centre for Neuromuscular and Neurological Disorders, University of Western Australia, Nedlands, Western Australia, Australia

[e]Department of Biomedical Engineering, The City College of the City University of New York, New York, NY, USA

[f]Behavioral Neurology Unit, National Institute of Neurological Disorders and Stroke, Bethesda, MD, USA

Abstract

Transcranial Direct Current Stimulation (tDCS) is a non-invasive, low-cost, well-tolerated technique producing lasting modulation of cortical excitability. Behavioral and therapeutic outcomes of tDCS are linked to the targeted brain regions, but there is little evidence that current reaches the brain as intended. We aimed to: (1) validate a computational model for estimating cortical electric fields in human transcranial stimulation, and (2) assess the magnitude and spread of cortical electric field with a novel High-Definition tDCS (HD-tDCS) scalp montage using a 4×1-Ring electrode configuration. In three healthy adults, Transcranial Electrical Stimulation (TES) over primary motor cortex (M1) was delivered using the 4×1 montage (4× cathode, surrounding a single central anode; montage radius ~3 cm) with sufficient intensity to elicit a discrete muscle twitch in the hand. The estimated current distribution in M1 was calculated using the individualized MRI-based model, and compared with the observed motor response across subjects. The response magnitude was quantified with stimulation over motor cortex as well as anterior and posterior to motor cortex. In each case the model data were consistent with the motor response across subjects. The estimated cortical electric fields with the 4×1 montage were compared (area, magnitude, direction) for TES and tDCS in each subject.

[*]Corresponding author at: Department of Neurology and Neuroscience, Weill Cornell Medical College, New York, NY, USA, dedwards@burke.org (D. Edwards).

We provide direct evidence in humans that TES with a 4×1-Ring configuration can activate motor cortex and that current does not substantially spread outside the stimulation area. Computational models predict that both TES and tDCS waveforms using the 4×1-Ring configuration generate electric fields in cortex with comparable gross current distribution, and preferentially directed normal (inward) currents. The agreement of modeling and experimental data for both current delivery and focality support the use of the HD-tDCS 4×1-Ring montage for cortically targeted neuromodulation.

Keywords

tDCS; TES; TMS; Targeted stimulation; Human head model; Electric fields

Introduction

Both transcranial electrical stimulation (TES)(Merton and Morton, 1980) and transcranial magnetic stimulation (TMS)(Barker et al., 1985) allow non-invasive electrical stimulation of the brain, with expanding applications in neuromodulation and electrotherapy. While significant sophistication has been applied to the refinement of transcranial magnetic stimulation for controlled targeting (Cohen et al., 1990; Deng et al., 2008; Ren et al., 1995; Roth et al., 2002; Ruohonen and Ilmoniemi, 1998), for transcranial electrical stimulation and transcranial direct current stimulation (tDCS), the prototypical electrode montages have remained “bipolar” (Merton and Morton, 1980; Merton et al., 1982; Nitsche and Paulus, 2000) or “unipolar” (Elbert et al., 1981; Lippold and Redfearn, 1964; Moliadze et al., 2010; Rossini et al., 1985). TES typically uses brief (~50 μs) voltage-controlled (>200 V) pulses, while tDCS is low voltage (~10–20 V) and current-controlled (~1–2 mA), applied for several minutes. Whereas TES can activate the corticospinal tract leading to a muscle twitch, tDCS does not evoke gross neurophysiological responses but rather is thought to alter the tone of neuronal excitability.

tDCS induces lasting biological effects (Edwards et al., 2009; Nitsche and Paulus, 2001) and is being currently explored to treat a range of neuropsychiatric disorders and facilitate rehabilitation, including after stroke (Hummel et al., 2005). The relative position and size of tDCS electrodes can shape the outcome of stimulation (Moliadze et al., 2010; Nitsche et al., 2007), but modeling and imaging studies suggest diffuse brain modulation (Bikson et al., 2010; Datta et al., 2009; Lang et al., 2005). The development of advanced tools for targeted non-invasive cortical neuromodulation, such as High-Definition tDCS (HD-tDCS), remains of significant interest to the clinical community.

Using high-resolution finite-element-method (FEM) computational models, we recently predicted that *High Definition* electrode arrays could be used to design sophisticated and targeted transcranial electrode montages (Datta et al., 2009; Minhas et al., 2010). For example, the *4×1-Ring* montage, with a center active electrode surrounded by 4 return electrodes forming a ‘ring’, could be used to focus transcranial current within a cortical area circumscribed by the ring (Datta et al., 2009). Despite promising results from pilot clinical trials (Borckardt et al., 2012; Minhas et al., 2010), it remains important to validate the

current delivery and focality of HD-tDCS. Though computational current-flow models are based on straightforward assumptions (e.g. Ohm's law), there is a dearth of direct prediction validation. TES has been used to map motor function since a response is evident only when sufficient current density penetrates primary motor cortex (M1) (Cohen and Hallett, 1988; Saypol et al., 1991), and results have been linked to brain electric fields using spherical models (Stecker, 2005).

The purpose of the present study was to provide physiological and anatomically-specific modeling evidence supporting focal brain activation by a HD 4×1-Ring electrode montage (HD-tDCS$_{4\times1}$). Since tDCS, does not induce an acute evoked response, we applied TES using suprathreshold pulses, which results in a quantifiable muscle response when current activates motor cortex efferent axons (Day et al., 1989; Merton and Morton, 1980). Quantification of evoked muscle response following TES using a 4×1-Ring montage (TES$_{4\times1}$; 140 mm^2 contact area per electrode) was used to verify brain stimulation magnitude and focality. Moreover, individualized MRI-derived computational models were able to distinguish the current density at M1 between subjects, based on stimulation intensity and position at the scalp. The models verified that current reaches the gray and white matter with comparable focality and directionality for TES$_{4\times1}$ and HD-tDCS$_{4\times1}$. These findings support the use of the 4×1 electrode montage for focal neuromodulation and electrotherapy.

Methods

Brain stimulation experiments

Participants—Three healthy participants (1 female, 2 male, 32–39 years of age) volunteered for the study. Written informed consent was obtained prior to the study, which had approval of the Institutional Review Board of the Burke Rehabilitation Hospital.

Positioning and set-up—During the experiment, subjects were comfortably seated with the forearms and hands resting on a pillow over the thighs. An EEG reference cap was positioned and worn throughout the experiment. To ensure that the cap had not moved during the experiment, the position was confirmed at the end of the session.

Transcranial electrical stimulation 4×1 montage (TES$_{4\times1}$)

Cap—The EEG cap (EasyCap, Brain Vision, Durham, NC; it is important to note that EasyCap electrode holders and electrodes are *not* suitable for stimulation) was gently secured on the head of each subject and positioned with Cz at the vertex, as measured using surface anatomical landmarks, and defined as the intersection of the nasion–inion and interaural lines.

Electrodes—TES$_{4\times1}$ was delivered with Sintered Ag/AgCl ring electrodes (EL-TP-RNG Sintered, StensBiofeedback Inc. San Rafael, CA, USA) using customized high-definition electrode holders with 12-mm outer diameter and 140-mm^2 gel contact area on the scalp (Minhas et al., 2010). The electrode casings were first injected with 1 mL of a sterile solution, containing 6% benzocaine and 0.2% benzethonium, which was worked into the scalp using a cotton swab. The electrode casings were then filled with >3 mL of Signa Gel

(Parker Laboratories; NJ, USA) into which the Ag/AgCl ring electrode was immersed. The cotton swab was used to adjust the gel and hair until the electrode resistance was less than 10 kΩ prior to stimulation. Each electrode was used for only 30 pulses and new electrodes were used for each subject. Electrodes were positioned with 1 anode at the center (C3), over approximately the hand motor cortex of the left hemisphere, and 4 cathodes as return electrodes in the adjacent EEG positions (FC5, FC1, CP5, CP1), forming a "ring" montage. This electrode arrangement was termed $TES_{4\times1}$, and was subsequently applied anterior (anode: FC3, cathodes: F5, F1, C5, C1), equating to 1 × radius of the ring (1-R), then further anterior at 2× radius (2-R) of the ring (anode: F3, cathodes: AF7, AFz, FC5, FC1), followed by posterior at 1-R (anode: CP3, cathodes: C5, C1, P5, P1) and 2-R (anode: P3, cathodes: CP5, CP1, PO7, POz; Fig. 3).

Stimulation—Electrical stimulation was performed using a constant voltage Cortical Stimulator (Model D185, Digitimer Ltd, UK, maximal output 1000 V/1.5 A) with single square-wave 50-μs pulses (0.1 A/μs rise time). As the Digitimer D185 is designed for conventional 2-channel stimulation, for $TES_{4\times1}$, a HD-$tDCS_{4\times1}$ Multi-Channel Stimulation Adaptor (Soterix Medical, New York, NY) was connected between the Digitimer D185 and the Ag/AgCl electrodes. The adaptor measured resistance prior to stimulation, and divided current during stimulation. It is important to emphasize that $TES_{4\times1}$ should only be applied with appropriate electrodes and hardware.

Transcranial magnetic stimulation (TMS)—TMS was applied with a figure-of-eight coil (outer diameter: 75 mm) delivered by a MagPro X100 stimulator (MagPro, MagVenture A/S, Farum Denmark) with the handle posterior (aligned in the para-sagittal plane) and rotated 45 degrees lateral. The coil was positioned over the site of the anode and flush with the cap (electrode removed), using a pre-marked reference on the scalp, in each of C3, FC3, F3, CP3 and P3 positions.

Electromyographic (EMG) recording—Pre-amplified bipolar surface EMG electrodes (1 -cm diameter, 2-cm inter-pole distance, ×1000 gain, band-pass filter 20–1000 Hz; Biometrics Ltd, UK) were taped over the belly of the right FDI muscle, recording the evoked muscle response to TMS and $TES_{4\times1}$ (motor evoked potential, MEP). EMG data were digitized at 2 kHz for 500 ms following each stimulus trigger and 100 ms pre-trigger, using a Micro1401 Acquisition system (Cambridge Electronic Design, Cambridge, UK). Subjects were instructed to maintain relaxation throughout the experiment, and EMG was monitored in real-time as biofeedback for the subject, and confirmed with post-analysis of pre-trigger EMG.

MEP waveform analysis—Peak-to-peak MEP amplitude of the non-rectified signal was calculated on individual waveforms using Spike 2 software (Cambridge Electronic Design, Cambridge, UK), and was reported as mean MEP amplitude for each stimulus intensity. MEP latency was measured for each epoch at the onset of the negative waveform deflection.

Experimental procedure

$TES_{4\times1}$—With electrodes positioned for motor cortex stimulation (anode C3), the constant voltage TES stimulator intensity was progressively increased (1–2 stimuli, 50–100 V increments, commencing at 50 V) until consistent MEPs of 0.3–0.5 mV were elicited. Five MEPs were collected at this site, before the electrodes were moved to the anterior, and then posterior positions (see above for exact location). For the sites away from M1, five stimuli were delivered at the same intensity or higher (to confirm the presence or absence of an evoked response in these positions). MEPs larger than 0.3–0.5 mV could be obtained in two of the subjects at C3. We progressively increased the intensity to achieve a plateau in MEP amplitude (not exceeding 2 mV). The higher intensity for the two subjects was additionally tested for presence or absence of MEP in the anterior and posterior positions.

TMS—Immediately following TES, the TMS coil was positioned over the C3 region, and the stimulus intensity was adjusted to elicit the same amplitude (0.3–0.5 mV) MEPs as during the TES. 10 MEPs were collected. Five stimuli were then delivered, in the anterior and posterior positions to test for the presence/absence of MEPs. For the two subjects able to attain greater than 0.3–0.5 mV in C3 position, TMS intensity was matched to elicit comparable maximal amplitude MEPs and was repeated in the anterior and posterior positions.

Computational models

MRI derived high-resolution model—We developed an individualized finite element (FE) head model to compare across the experimentally evaluated $TES_{4\times1}$ (see below) electrode montages. In addition, results were compared with a $HD\text{-}tDCS_{4\times1}$ model. The head models were created from 1 mm^3 resolution T1-weighted MRI scans of each subject. Using a combination of tools: a) FSL from the Functional MRI of the Brain (FMRIB) Software Library (United Kingdom) and b) Simpleware (Simpleware Ltd., United Kingdom), the subject's head was segmented into compartments representing gray matter, white matter, cerebrospinal fluid (CSF), skull, scalp, and air (Custom Segmentation, Soterix Medical NY, USA; Fig. 1). The finite element (FE) mesh generated from the segmented compartments was exported to COMSOL Multiphysics 3.5a (Burlington, Massachusetts) for computation of electric fields (Datta et al., 2009).

TES model—The quasi-static approximation enables Maxwell's equations to be simplified by ignoring the capacitive, inductive, and wave propagation effects (Bossetti et al., 2008). For DC models, the absence of the frequency component makes this approximation valid. Thus typically, the standard Laplace equation with purely conductive properties is solved (Datta et al., 2009; Miranda et al., 2006; Wagner et al., 2007):

$$\nabla.(\sigma\nabla V)=0 \quad (1)$$

where σ: represents tissue conductivity; and V: represents electric potential. However for TES, the stimulator generates rapidly rising short duration pulses exhibiting wide spectral content. In addition, the dielectric properties (conductivity and permittivity) of tissue exhibit

strong frequency dependence (Gabriel et al., 1996). Thus the standard Laplace equation is modified to incorporate reactive components:

$$\nabla \cdot (\sigma + j\omega\varepsilon)\nabla V = 0 \quad (2)$$

where ε: permittivity (F/m) which represents the product of the relative permittivity, ε_r and the free space permittivity, ε_0; and ω: angular frequency.

The Fourier magnitude spectrum of a typical TES square pulse (T = 50 μs) results in power concentrated from 0 to 20 kHz (where 20 kHz is 1/T; the first zero crossing). Additionally, since the TES stimulator generates voltage controlled pulses, the shape and the amplitude of the current/electric field (EF) waveform delivered to the tissue is distorted (Merrill et al., 2005). We therefore considered tissue properties (conductivity and permittivity) at 10 kHz (half of the first zero crossing). The real component of Eq. (2) dominates the solution at 10 kHz (ε_r varies from 1e4–1e5; (Gabriel et al., 1996)) such that we approximated the solution for V by using the quasi-static simplification at 10 kHz (as implemented previously; (Roth et al., 1991)).

In the context of this study's goals, our primary modeling objective was to consider and compare the spatial distribution of induced cortical current flow for the $TES_{4\times1}$ and HD-$tDCS_{4\times1}$ cases, for which a comparison between the 10 kHz and DC case is rational. In contrast, a detailed modeling study of neuronal activation would require consideration of electrode capacitances and non-linearity (Merrill et al., 2005), and solving of the Laplace equation for each frequency (see Fourier-FEM approach, (Butson and McIntyre, 2005)), followed by detailed biophysical modeling using the activation function/multi-compartment modeling with distributed voltage-gated ion channels considering different cell classes (McIntyre et al., 2004; Radman et al., 2009). Nonetheless, we use the peak cortical electrical field at 10 kHz as a first approximation of relative neuronal activation in motor regions; such that regions with low electric field would be unlikely to be activated, regions with high electric field would be likely to be activated, and regions with comparable electric fields may be activated to a similar extent. This approach is substantiated *a priori* by the well-established sensitivity to electric field of bent and terminating processes (Rattay, 1986) as expected in tortuous cortex, as well as sensitivity of compact neurons (Bikson et al., 2004; Joucla and Yvert, 2009; Rattay, 1986); and *a posteriori* from correlation with our experimental series.

We modeled the following $TES_{4\times1}$ electrode montages representing the experimental montages used in this study (Fig. 1): Anterior (1-R and 2-R); (2) Motor (C3) and (3) Posterior (1-R and 2-R). The anode electrode was energized to 1000 V (electrode boundary) and ground was applied to the cathode electrodes.

The following isotropic electrical conductivities (in S/m) corresponding to 10 kHz were assigned: gray matter: 0.1; white matter: 0.07; CSF: 1.65; skull: 0.01; scalp: 0.006; and air: 1e-15 (Gabriel et al., 1996).

Data analysis for $TES_{4\times1}$ physiology and modeling—The electric field was modeled at M1 for all experimental conditions (i.e. different voltages for motor cortex

stimulation, and for non-motor stimulation) and are reported as: (1) cortical surface EF peak and range measured from the M1 gyrus crown, where *C3 peak* is maximal cortical value beneath the C3 electrode (from 1 cm^2 sample), and *M1 range* is the minimum to maximum values along the length of the precentral gyrus crown between the inter-hemispheric and lateral fissures, and (2) cortical and white matter EF range, reported as the minimum to maximum values from a sagittal slice (1 mm) through the precentral gyrus at C3, encompassing the entire cortical region of M1 (anterior and posterior banks, gyrus crown, and white matter to the depth of the anterior and posterior sulci). The electric field range was recorded from the model by decreasing the scale of the intensity plots in the region of interest (ROI); the upper limit defined as the minimum intensity at which all values of the electric field present across the ROI were covered; and the lower limit defined as the maximal intensity at which no value of the electric field present in the ROI was covered.

HD-tDCS$_{4\times1}$ model—The typical model settings as established previously were used (Datta et al., 2009; Miranda et al., 2006; Wagner et al., 2007), and the aforementioned TES$_{4\times1}$ motor montage was solved for HD-tDCS$_{4\times1}$. This montage corresponds to the 4×1-Ring HD-tDCS configuration (at a slightly wider center active to outer return distance than Datta and colleagues; (Datta et al., 2009)). The following isotropic electrical conductivities (in S/m) were assigned: gray matter: 0.276; white matter: 0.126; CSF: 1.65; skull: 0.01; scalp: 0.465; and air: 1e-15 (Datta et al., 2009; Wagner et al., 2007). Current density corresponding to 1 mA total current (current density boundary) was applied at the anode, as is typically used for tDCS, and ground was applied to the cathodes.

Model solution description and justification—TES$_{4\times1}$ and HD-tDCS$_{4\times1}$ model montages corresponded to the conditions tested experimentally. All disk electrodes were 12 mm in diameter as used experimentally. The gel and electrodes had the following electrical conductivities (in S/m) respectively: 0.3 and 5.9e7. All other external surfaces (barring the anode and the cathode electrode surfaces) were treated as insulated. The models comprised >10,000,000 second order tetrahedral elements with >15,000,000 degrees of freedom. The Laplace equation (Eq. (1)) was solved and induced cortical surface electric field (EF) magnitude or cortical surface normal directional electric field maps for the different electrode configurations were determined.

Results

High-resolution computational models predict that using the High-Definition 4×1-ring electrode montage, current can be delivered to the area of cortex circumscribed by the ring. The overall goal of the experimental and modeling work in the present study, was to validate both the intensity and focality of current delivery to cerebral cortex using the High-Definition 4×1-Ring Electrode Montage. Because weak DC stimulation, as used in tDCS, does not induce a manifest physiological response, we used TES$_{4\times1}$ with high-voltage pulses to elicit evoked motor responses that served as a substrate to quantify current delivery and focality. MRI-derived subject-specific modeling of generated cortical electric fields was matched with the experimental data.

Validation of stimulation intensity: Subject-specific delivery of electric field intensity to motor cortex

To assess whether predicted cortical fields were consistent with the observed motor response experimentally, we tested two stimulus intensities in each subject: (a) with a variable stimulus input, adjusted to give a comparable motor response across subjects (0.3–0.5 mV MEP), and (b) consistent stimulus input (600 V), giving a variable response across subjects. In each case, subject-specific model predictions were validated by experimental measurement of MEP responses.

Stimulus adjusted for 0.3–0.5 mV MEPs—In all three subjects, the stimulus intensity required to elicit comparable amplitude MEPs at C3 was different, as predicted by the models (Fig. 2). Subject C required the lowest stimulus intensity at 400 V (current=709±0 mA; MEP amplitude=0.46±0.08 mV), which corresponded in the Subject C model to a primary motor cortex EF peak around 150 V/m (C3 peak=144 V/m; C3 sagittal range=70–100 V/m; M1 range=46–146 V/m). Subject B required higher stimulus intensity at 480 V (input current 1138±0 mA; MEP amplitude=0.45±0.12 mV) that corresponded in the Subject B model to a primary motor cortex EF peak around 230 V/m (C3 peak=192 V/m, C3 sagittal range=72–152 V/m, M1 range= 29–228 V/m). Subject A required the highest stimulus intensity at 1000 V (input current=1738±1 mA; MEP amplitude= 0.35± 0.07 mV) that corresponded in the Subject A model to a primary motor cortex EF peak of around 160 V/m(C3 peak=163 V/m, C3 sagittal range=65–90 V/m, M1 range=50–163 V/m). Notably, a greater than two-fold variation in applied voltage to the scalp across subjects, resulted in a comparable electric field predicted in the motor cortex. Though evoked neuronal threshold is highly dependent on the neuronal compartment target (Rattay, 1986), ongoing activity (Reato et al., 2010), pulse waveform and EF direction (Radman et al., 2009), neuronal activation at 100–200 V/m is broadly consistent with previous animal and modeling studies (Radman et al., 2009; Saypol et al., 1991; Thielscher and Kammer, 2002).

For each subject, the C3 electrode was confirmed to be over M1 approximately 1 cm lateral to the hand knob in the sagittal plane (identified using structural MRI; (Yousry et al., 1997)). Although responses from the hand can readily be evoked from stimulation several centimeters along M1, the most responsive area for the index finger is on the lateral side of the hand knob in healthy human subjects (Thielscher and Kammer, 2002). Our findings across subjects showed that EF from an M1 sagittal slice centered at C3, peaked at 90–152 V/m then attenuated medially ~50% by the center of the hand knob (total distance 2 cm), peaking at 30–86 V/m (for central C3 sagittal range, see Table 1; for central hand knob sagittal range, Subject A=55–60 V/m, Subject B= 24–30 V/m, and Subject C=64–86 V/m).

Constant 600 V input stimulus—With 600 V delivered over the scalp at primary motor cortex, the predicted cortical field in each subject was commensurate with the magnitude of evoked response. No response could be elicited in Subject A, consistent with the low predicted EF in primary motor cortex (C3 input stimulus=600 V/950±104 mA, C3 peak=96V/m, C3 sagittal range=39–54 V/m, M1 range=30–96 V/m, MEP amplitude <0.00 mV). High predicted M1 cortical electric fields in Subjects C and B corresponded to large evoked responses to stimulation (Subject C: Stimulus intensity=600 V/1168±2 mA, C3

peak=216 V/m, C3 sagittal range=108–150 V/m, M1 range=69–219 V/m, MEP amplitude= 1.37±0.04 mV; Subject B: Stimulus intensity=600 V/1565±7 mA, C3 peak=240 V/m, C3 sagittal range=90–190 V/m, M1 range= 36–284 V/m, MEP amplitude=1.77±0.01 mV).

We further considered the robustness of model predictions to tissue conductivity; specifically noting the higher resistivity of skin than skull indicated in the literature at 10 kHz (skin ~0.006 S/m, skull ~0.01 S/m; (Gabriel et al., 1996)), we modeled a scalp conductivity of 0.01 S/m. The peak electric field in each case increased and by a comparable ratio of ~40%, ~30%, and ~60% in Subjects A, B, and C, respectively, and the spatial distribution did not change (note: the 4×1 remains focal across tissue properties, even simulating a homogenous head; (Datta et al., 2009)). Especially, given our inter-subject model validation relies on relative responsiveness, this finding supports the robustness of our modeling conclusions.

Validation of stimulation focality: Targeting of electric field within the 4×1-ring

Experimental responses were used to validate modeled targeting of cortical electric fields which predicted, across all subjects (independent of individual anatomy) significant electric field decrease at 1-R (corresponding to the cortex under the outer electrode ring radius) and minimal electric field at 2-R (Table 1). In each of the three subjects the same stimulus intensity required to elicit 0.3–0.5 mV MEPs at C3 could only weakly elicit responses from 1-R (i.e. when the montage was moved from C3 anteriorly or posteriorly ~3cm, radius of cathode ring). Two of the subjects required either a muscle contraction (Subject B) or higher stimulus intensity (Subject C) to generate MEPs at this distance. No responses could be obtained from the 2-R position in either direction (i.e. ~6 cm anterior or posterior to M1 hand area) even at higher-intensities. The physiologic findings were consistent with the models showing that negligible current reaches M1 from the 2-R position, while a fractional amount reaches it from 1-R in the physiologic range for activation. Fig. 3 shows the models and sample representative MEP responses from one subject (Subject A) corresponding to the different scalp stimulation sites.

In summary, the $TES_{4\times1}$ experimental data are consistent with model data showing that electric field reaching the cortex is reduced to <30% by the circumference of the electrode ring (1-R) and <5% at double that distance (2-R). Movement of the montage the distance of the ring radius (~3 cm) in either the anterior or posterior direction, results in weak current reaching M1, while movement twice that distance results in minimal current.

Comparison with transcranial magnetic stimulation—Transcranial magnetic stimulation showed comparable amplitude evoked responses as $TES_{4\times1}$ at each of the stimulus locations, indicating that current spread from the two techniques (TMS and $TES_{4\times1}$) could not be distinguished at this spatial resolution. The same TMS intensity required to elicit 0.3–0.5mV MEPs at C3, when applied at 1-R could only weakly activate M1 and at 2-R could not activate M1 (leading to an evoked response). In subject B, this was true even with higher stimulus intensity at 2-R. As with $TES_{4\times1}$, Subject A required the highest stimulation intensity for equivalent size MEPs at C3 (Subjects A = 60% MSO, 0.37 ± 0.03 mV; Subject B = 30% MSO, 0.44 ± 0.18 mV, Subject C = 32% MSO, 0.39±0.09

mV). Again, similar to $TES_{4\times1}$, at the 1-R position with this intensity, TMS could elicit a small response for Subject A at rest (0.07 ±0.03 mV at FC3, 0.05 ±0.02 mV at CP3, Fig. 4), but for Subject B and Subject C, only if a muscle contraction was performed during stimulation (Subject B 10% MVIC = 0.52 ±0.14 mV at FC3, 0.28±0.04 mV at CP3; Subject C 10% MVIC = 0.14±0.02 mV at FC3, 0.14 ± 0.03 mV at CP3). At the 2-R positions no responses were obtained in any of the subjects (Subject A < 0.00 mVatF3,<0.00 mVatP3; Subject B<0.00 mV at F3, <0.00 mV at P3; Subject C = <0.00mV at F3, <0.00 mV at P3). We also considered latency differences between TMS and $TES_{4\times1}$ with comparable MEP amplitude (0.3–0.5mV) at C3. Mean MEP latency with $TES_{4\times1}$ was ~1–2 ms shorter than TMS for each subject (Subject A: $TES_{4\times1}$=23.4±0.5 ms; TMS=24.4±0.3 ms; Subject B: $TES_{4\times1}$=24.3±0.3 ms, TMS=26.2±0.2 ms; Subject C: $TES_{4\times1}$= 23.0±0.3 ms, TMS=23.8±0.3 ms).

Computational model: Low intensity DC over primary motor cortex

The evoked motor response with $TES_{4\times1}$ was used here as evidence for transcranial currents penetrating the brain with the 4×1 montage and the lack of response with stimulation anterior or posterior to motor cortex supports that minimal current exceeds the periphery of the electrode ring. These findings give credence to the accuracy of the models for $TES_{4\times1}$. We next used computational models to predict the cortical current density from HD-$tDCS_{4\times1}$ as well as the relative focality in relation to $TES_{4\times1}$ (normalized to peak cortical induced fields).

HD-$tDCS_{4\times1}$ intensity and targeting—The modeling data show that, like $TES_{4\times1}$, HD-$tDCS_{4\times1}$ (1mA) current is delivered to the brain below the anode with the electric field reduced to <30% of peak value at the ring perimeter. The results for each subject are as follows; Subject A: C3 peak=0.11 V/m, C3 sagittal range=0.05–0.08 V/m; M1 range= 0.00–0.12 V/m; Subject B: C3 peak=0.26 V/m, C3 sagittal range=0.11–0.23 V/m; M1 range= 0.102–0.35 V/m; Subject C: C3 peak=0.18 V/m, C3 sagittal range= 0.16–0.21 V/m, M1 range=0.10–0.25 V/m. Of note, for both $TES_{4\times1}$ and HD-$tDCS_{4\times1}$, there was penetration beyond cortex and into white matter.

Comparison of relative focality using the same C3 centered montage applying either $TES_{4\times1}$ or HD-$tDCS_{4\times1}$ stimulation indicates that in both cases, current flow is largely restricted within the cortex circumscribed by the ring. $TES_{4\times1}$ has slightly greater focality (Fig. 5; A.1, B.1) and less penetration depth (Fig. 5; A.2, B.2) than HD-$tDCS_{4\times1}$, when expressed relative to individual peak intensities. Topographically, the most highly activated gyri were comparable for both cases (Fig. 5; A.1b, B.1b).

Normal current profile—We further considered the directionality of current flow across the cortex (Datta et al., 2008) since the direction of current flow across the gray matter is considered to influence the action of stimulation (Nitsche and Paulus, 2000). For both $TES_{4\times1}$ and HD-$tDCS_{4\times1}$, the profile of activation was not substantially different when considering normal current (orthogonal to the scalp) (Fig. 5 A.1a, B.1a). This finding is readily reconcilable with the concept that inside the ring, current is dominantly inward (as

opposed to outward or tangential), while the return of outward current outside the ring is diffuse and thus weak (Datta et al., 2008).

Discussion

The rationale for this study arose from two poorly understood aspects of tDCS. Firstly, the intensity of current that reaches and affects cortex below the electrodes is difficult to determine, and is typically inferred from physiologic outcomes (often recorded in the post-stimulation period) such as fMRI, EEG or MEP responses, which are not necessarily linear (or even monotonic) with local current intensity, or from behavioral changes, where the relationship with regional current flow is yet less clear. This is because, unlike TMS, tDCS itself does not produce an overt response. Secondly, recent modeling and imaging data show that while some current does penetrate the cortex, using conventional tDCS-montages with large electrode-pads, current spreads far across the cerebrum with maximum effect often not below the electrode pads as assumed. Indeed, this last finding encourages the development of targeted tDCS montages using High-Definition (HD) electrodes. To address fundamental questions related to tDCS dose design and specifically validate focalized tDCS, we used TES to verify MRI-derived current flow modeling.

Our findings in the context of existing non-invasive electrical stimulation paradigms

Transcranial direct current stimulation is an emerging therapy for neurological disorders with an attractive safety, cost, side-effect, and customization profile. In this last regard, tDCS can be adjusted for specific experimental studies or therapeutic applications through the electrode montage. Conventional tDCS uses relatively large (e.g. 5×5 cm^2) sponge electrodes, with the anode positioned over cortical regions to increase excitability, while the cathode is positioned over cortical regions to reduce excitability (Nitsche and Paulus, 2000; Nitsche et al., 2008). Behavioral correlates and neurophysiological probes (for sensory/motor regions) provide some support for this heuristic approach to electrode montage design, at least when averaging across individuals (Antal et al., 2004). However, modeling (Datta et al., 2009; Sadleir et al., 2010) and imaging (Baudewig et al., 2001; Lang et al., 2005) studies of tDCS suggest that conventional tDCS electrode montages using large, damp sponge electrodes result in very diffuse brain current flow, with areas of clustering (hot spots), and the target area is ineffectively pervaded. Though the position and size of sponge electrodes can *shape* the effects of tDCS (Moliadze et al., 2010; Nitsche et al., 2007), overall current flow presumably remains diffuse (Bikson et al., 2010). The recent development of High-Definition electrodes allows for safe and comfortable transcranial stimulation with DC currents, though a smaller scalp surface area than conventional pad electrodes (Minhas et al., 2010). Modeling studies predict that High-Definition electrodes in the 4×1 montage (HD-$tDCS_{4\times1}$) provide further benefit of well controlled (focalized) and unifocal cortical activation (Datta et al., 2008). The validation of the HD-$tDCS_{4\times1}$ montage is thus of broad interest in non-invasive neuromodulation and electrotherapy, and suggests an advancement in the methods and technology for non-invasive brain stimulation.

Support for the High-Definition 4 ×1-Ring montage in tDCS

Because DC current does not directly produce neuronal firing, in this report we applied TES – triggering a motor response - through the High-Definition 4×1 montage ($TES_{4\times1}$). Using an integration of modeling and experimental approaches, we were able to then: 1) Estimate the peak magnitude (efficacy) of current that is delivered using the 4× 1 montage; and 2) Validate the spatial specificity (targeting) of this montage.

Under the assumptions of comparable electric field threshold for cortical activation across subjects, the model predicted significant (>two-fold) difference across subjects in M1 electric fields using the same 4×1 montages centered over C3. These predictions were validated quantitatively using both fixed MEP-amplitude response and fixed stimulation voltage experiments. To our knowledge this is the first use of MRI-derived forward modeling to resolve individual sensitivity with high precision. Though we did not model membrane polarization by electric fields explicitly, the electric fields predicted for supra-threshold stimulation (100–200 V/m) are comparable with previous modeling and experimental measurements for short pulses in vitro (Radman et al., 2009). Our model predictions of cortical EF in humans are also broadly consistent with previous studies, despite variations in sampling area (location, depth, size) and current direction. Whereas previous work using spherical models (Saypol et al., 1991; Thielscher and Kammer, 2002) shows peak EF typically below 100 V/m, using high precision anatomical models (gyri/sulci precise), we show the peak EF to be above 100 V/m for each subject. Accounting for the intricate pattern of CSF distribution identified with high precision models, EF ‘hotspots’ are evident, and might explain peak values exceeding 200V/m in some cases.

We showed that $TES_{4\times1}$ results in focal brain activation, with peak EF near the center active electrode, reduction in intensity by ~30% at the ring perimeter, and no significant electric fields (relative to the peak) outside the ring. Across subjects and for each stimulation position (anode: C3, FC3, F3, CP3, or P3), MEP response was consistent with the model prediction. Though the spatial profile was influenced by cortical topography, generally this can be approximated as a rate of decay along the cortical surface with a space constant equal to 1 ring-radius (1-R).

The use of TMS in this study was intended to inform whether any response at stimulus sites anterior and posterior to primary motor cortex with $TES_{4\times1}$ could be explained by current spread, acknowledging that electric field orientation is different, and with the assumption that TMS has greater stimulation precision than $TES_{4\times1}$. For example, an MEP response from $TES_{4\times1}$ but not TMS would infer that 4×1 current is spreading to neighboring primary cortex, rather than elements of primary cortex being below the stimulation site. Stimulus intensity was thus reduced (0.3–0.5 mV MEP response) to minimize current spread effects. However, at the spatial resolution tested (1-R), we could not distinguish the relative focality between $TES_{4\times1}$ and TMS. The 1–2 ms shorter MEP latency following $TES_{4\times1}$ relative to TMS is consistent with previous studies of bipolar TES and TMS (Day et al., 1989; Rothwell et al., 1991). This may reflect earlier descending volleys from direct corticospinal activation in the case of $TES_{4\times1}$, and suggests that physiologic effects from the HD 4×1 montage can extend beyond cortical interneurons.

Broader implications for rational dose design

Computational modeling studies predict that conventional bipolar stimulation using electrode pads (M1-supraorbital montage) does not produce maximum cortical electric fields below the electrode pads as originally intended. However, evoked potential data provides evidence that corticomotor excitability can change directly below the electrode pad (Nitsche and Paulus, 2000), and subsequent studies have shown motor behavioral improvement with this montage (Hummel et al., 2006; Nitsche et al., 2003). The extent to which a more circumscribed field can change clinical effects remains to be determined, and investigations are presently underway in our laboratory and others. As HD-tDCS$_{4\times1}$ is conventionally applied, with ~4–7 cm ring radius, the peak cortical electric field is comparable to conventional tDCS, thus clinical differences may result from; 1) which brain regions are not stimulated by tDCS – where diffuse current flow may influence side-effects and complex (ant)agonistic regional interactions; 2) macroscopic variation in current flow patterns within the target (e.g. direction, uniformity, consistency across individuals). These issues are highly anatomy dependent, and need to be resolved on a per-indication and montage basis. Interestingly, the HD-tDCS$_{4\times1}$ montage centered over M1, leads to a more profound and lasting change in motor evoked potential amplitude than bipolar stimulation, albeit with different onset time-course (Kuo et al., 2012).

The results of the present study show that the High-Definition 4×1 montage can be used to deliver focal electrical stimulation, ranging from pulsed to DC waveform, to discrete and targeted brain regions. Though frequency-dependent tissue properties are predicted to moderately affect focalization using high-frequency (TES) versus DC waveforms, in all cases maximum cortical activation (including normal/inward excitatory current flow) is circumscribed by the ring diameter. Indeed, a feature of the 4×1 ring configuration, as opposed to conventional bipolar montages, is restriction of peak activation under the active electrode, even across large variations in tissue conductivity ((Datta et al., 2009); Fig. 5). The HD-4×1 montage can thus be explored for focalizing a range of waveforms, including using tDCS, transcranial alternating current stimulation (tACS) (Antal et al., 2008), transcranial Pulsed Current Stimulation (tPCS) and its derivatives such as Cranial Electrotherapy Stimulation (Kirsch and Smith, 2000), and transcranial high-frequency random noise stimulation (tRNS)(Terney et al., 2008). Whether higher frequencies can in fact be leveraged to increase focality still further (Fig. 5) in a clinically meaningful manner is a compelling open question.

We note that High-Definition-tDCS could be delivered using many different positions and number of electrodes; with each montage optimized for a specific clinical or experimental objective (Dmochowski et al., 2011). Even using the 4×1-ring selected in the present study, the depth, focality, and intensity of stimulation can be altered by changing the ring diameter. In the extreme case, the belt configuration, can result in broad cortical penetration (Rossini et al., 1985; Saypol et al., 1991).

Computational forward models of increasing sophistication have been developed to explain clinical results and develop new waveforms (Bikson and Datta, 2012). Yet there is a dearth of direct model validation. The TES results thus provide general validation for the modeling approach used in this study, and a quantitative method to access other modeling approaches.

In summary, our findings support High-Definition tDCS using the 4×1-Ring configuration as a technique for delivering focal cortical stimulation in a predictable and adjustable manner. This represents a paradigm shift for therapeutic tDCS intending to target specific cortical areas. For primary motor cortex stimulation, the area of effective stimulation is probably limited to the targeted somatotopic region, without substantial spread to other primary motor or non-motor areas. Our results suggest that the focality holds for stimulation of non-motor cortical areas, and thus may be useful for targeted HD-tDCS$_{4\times1}$ of other cortical areas such as temporal, occipital, pre-frontal, and cerebellar cortex. The physiological effects of HD-tDCS$_{4\times1}$ require further investigation, especially the relationship to potential therapeutic benefit, but HD-tDCS may combine the advantages of conventional tDCS and repetitive TMS (rTMS) techniques (practicality, safety and focality).

Supplementary Material

Refer to Web version on PubMed Central for supplementary material.

References

Antal A, Nitsche MA, Kincses TZ, Kruse W, Hoffmann K, Paulus W. Facilitation of visuo-motor learning by transcranial direct current stimulation of the motor and extrastriate visual areas in humans. Eur. J. Neurosci. 2004; 19:2888–2892. [PubMed: 15147322]

Antal A, Boros K, Poreisz C, Chaieb L, Terney D, Paulus W. Comparatively weak after-effects of transcranial alternating current stimulation (tACS) on cortical excitability in humans. Brain Stimul. 2008; 1:97–105. [PubMed: 20633376]

Barker AT, Jalinous R, Freeston IL. Non-invasive magnetic stimulation of human motor cortex. Lancet. 1985; 1:1106–1107. [PubMed: 2860322]

Baudewig J, Nitsche MA, Paulus W, Frahm J. Regional modulation of BOLD MRI responses to human sensorimotor activation by transcranial direct current stimulation. Magn. Reson. Med. 2001; 45:196–201. [PubMed: 11180425]

Bikson M, Datta A. Guidelines for precise and accurate computational models of tDCS. Brain Stimul. 2012; 5:430–431. [PubMed: 21782547]

Bikson M, Inoue M, Akiyama H, Deans JK, Fox JE, Miyakawa H, Jefferys JG. Effects of uniform extracellular DC electric fields on excitability in rat hippocampal slices in vitro. J. Physiol. 2004; 557:175–190. [PubMed: 14978199]

Bikson M, Datta A, Rahman A, Scaturro J. Electrode montages for tDCS and weak transcranial electrical stimulation: role of “return” electrode's position and size. Clin. Neurophysiol. 2010; 121:1976–1978. [PubMed: 21035740]

Borckardt JJ, Bikson M, Frohman H, Reeves ST, Datta A, Bansal V, Madan A, Barth K, George MS. A pilot study of the tolerability and effects of high-definition transcranial direct current stimulation (HD-tDCS) on pain perception. J. Pain. 2012; 13:112–120. [PubMed: 22104190]

Bossetti CA, Birdno MJ, Grill WM. Analysis of the quasi-static approximation for calculating potentials generated by neural stimulation. J. Neural Eng. 2008; 5:44–53. [PubMed: 18310810]

Butson CR, McIntyre CC. Tissue and electrode capacitance reduce neural activation volumes during deep brain stimulation. Clin. Neurophysiol. 2005; 116:2490–2500. [PubMed: 16125463]

Cohen LG, Hallett M. Methodology for non-invasive mapping of human motor cortex with electrical stimulation. Electroencephalogr. Clin. Neurophysiol. 1988; 69:403–411. [PubMed: 2451587]

Cohen LG, Roth BJ, Nilsson J, Dang N, Panizza M, Bandinelli S, Friauf W, Hallett M. Effects of coil design on delivery of focal magnetic stimulation. Technical considerations. Electroencephalogr. Clin. Neurophysiol. 1990; 75:350–357. [PubMed: 1691084]

Datta A, Elwassif M, Battaglia F, Bikson M. Transcranial current stimulation focality using disc and ring electrode configurations: FEM analysis. J. Neural Eng. 2008; 5:163–174. [PubMed: 18441418]

Datta A, Bansal V, Diaz J, Patel J, Reato D, Bikson M. Gyri-precise head model of transcranial DC stimulation: improved spatial focality using a ring electrode versus conventional rectangular pad. Brain Stimul. 2009; 2:201–207. [PubMed: 20648973]

Day BL, Dressler D, Maertens de Noordhout A, Marsden CD, Nakashima K, Rothwell JC, Thompson PD. Electric and magnetic stimulation of human motor cortex: surface EMG and single motor unit responses. J. Physiol. 1989; 412:449–473. [PubMed: 2489409]

Deng ZD, Peterchev AV, Lisanby SH. Coil design considerations for deep-brain transcranial magnetic stimulation (dTMS). Conf. Proc. IEEE Eng. Med. Biol. Soc. 2008; 2008:5675–5679. [PubMed: 19164005]

Dmochowski JP, Datta A, Bikson M, Su Y, Parra LC. Optimized multi-electrode stimulation increases focality and intensity at target J. Neural Eng. 2011; 8:046011.

Edwards DJ, Krebs HI, Rykman A, Zipse J, Thickbroom GW, Mastaglia FL, Pascual-Leone A, Volpe BT. Raised corticomotor excitability of M1 forearm area following anodal tDCS is sustained during robotic wrist therapy in chronic stroke. Restor. Neurol. Neurosci. 2009; 27:199–207. [PubMed: 19531875]

Elbert T, Lutzenberger W, Rockstroh B, Birbaumer N. The influence of low-level transcortical DC-currents on response speed in humans. Int J. Neurosci. 1981; 14:101–114. [PubMed: 7263138]

Gabriel S, Lau RW, Gabriel C. The dielectric properties of biological tissues: II. Measurements in the frequency range 10 Hz to 20 GHz. Phys. Med. Biol. 1996; 41:2251–2269. [PubMed: 8938025]

Hummel F, Celnik P, Giraux P, Floel A, Wu WH, Gerloff C, Cohen LG. Effects of non-invasive cortical stimulation on skilled motor function in chronic stroke. Brain. 2005; 128:490–499. [PubMed: 15634731]

Hummel F, Voller B, Celnik P, Floel A, Giraux P, Gerloff C, Cohen L. Effects of brain polarization on reaction times and pinch force in chronic stroke. BMC Neurosci. 2006; 7:73. [PubMed: 17083730]

Joucla S, Yvert B. The “mirror” estimate: an intuitive predictor of membrane polarization during extracellular stimulation. Biophys. J. 2009; 96:3495–3508. [PubMed: 19413956]

Kirsch DL, Smith RB. The use of cranial electrotherapy stimulation in the management of chronic pain: a review. NeuroRehabilitation. 2000; 14:85–94. [PubMed: 11455071]

Kuo HI, Bikson M, Datta A, Minhas P, Paulus W, Kuo MF, Nitsche MA. Comparing cortical plasticity induced by conventional and high-definition 4×1 ring tDCS: a neurophysiological study. Brain Stimul. 2012

Lang N, Siebner HR, Ward NS, Lee L, Nitsche MA, Paulus W, Rothwell JC, Lemon RN, Frackowiak RS. How does transcranial DC stimulation of the primary motor cortex alter regional neuronal activity in the human brain? Eur. J. Neurosci. 2005; 22:495–504. [PubMed: 16045502]

Lippold OC, Redfearn JW. Mental changes resulting from the passage of small direct currents through the human brain. Br. J. Psychiatry. 1964; 110:768–772. [PubMed: 14211693]

McIntyre CC, Grill WM, Sherman DL, Thakor NV. Cellular effects of deep brain stimulation: model-based analysis of activation and inhibition. J. Neurophysiol. 2004; 91:1457–1469. [PubMed: 14668299]

Merrill DR, Bikson M, Jefferys JG. Electrical stimulation of excitable tissue: design of efficacious and safe protocols. J. Neurosci. Methods. 2005; 141:171–198. [PubMed: 15661300]

Merton PA, Morton HB. Stimulation of the cerebral cortex in the intact human subject. Nature. 1980; 285:227. [PubMed: 7374773]

Merton PA, Hill DK, Morton HB, Marsden CD. Scope of a technique for electrical stimulation of human brain, spinal cord, and muscle. Lancet. 1982; 2:597–600. [PubMed: 6125739]

Minhas P, Bansal V, Patel J, Ho JS, Diaz J, Datta A, Bikson M. Electrodes for high-definition transcutaneous DC stimulation for applications in drug delivery and electrotherapy, including tDCS. J. Neurosci. Methods. 2010; 190:188–197. [PubMed: 20488204]

Miranda PC, Lomarev M, Hallett M. Modeling the current distribution during transcranial direct current stimulation. Clin. Neurophysiol. 2006; 117:1623–1629. [PubMed: 16762592]

Moliadze V, Antal A, Paulus W. Electrode-distance dependent after-effects of transcranial direct and random noise stimulation with extracephalic reference electrodes. Clin. Neurophysiol. 2010; 121:2165–2171. [PubMed: 20554472]

Nitsche MA, Paulus W. Excitability changes induced in the human motor cortex by weak transcranial direct current stimulation. J. Physiol. 2000; 527:633–639. [PubMed: 10990547]

Nitsche MA, Paulus W. Sustained excitability elevations induced by transcranial DC motor cortex stimulation in humans. Neurology. 2001; 57:1899–1901. [PubMed: 11723286]

Nitsche MA, Schauenburg A, Lang N, Liebetanz D, Exner C, Paulus W, Tergau F. Facilitation of implicit motor learning by weak transcranial direct current stimulation of the primary motor cortex in the human. J. Cogn. Neurosci. 2003; 15:619–626. [PubMed: 12803972]

Nitsche MA, Doemkes S, Karakose T, Antal A, Liebetanz D, Lang N, Tergau F, Paulus W. Shaping the effects of transcranial direct current stimulation of the human motor cortex. J. Neurophysiol. 2007; 97:3109–3117. [PubMed: 17251360]

Nitsche MA, Cohen LG, Wassermann EM, Priori A, Lang N, Antal A, Paulus W, Hummel F, Boggio PS, Fregni F, et al. Transcranial direct current stimulation: state of the art 2008. Brain Stimul. 2008; 1:206–223. [PubMed: 20633386]

Radman T, Ramos RL, Brumberg JC, Bikson M. Role of cortical cell type and morphology in subthreshold and suprathreshold uniform electric field stimulation in vitro. Brain Stimul. 2009; 2:215–228. (228 e211–213). [PubMed: 20161507]

Rattay F. Analysis of models for external stimulation of axons. IEEE Trans. Biomed. Eng. 1986; 33:974–977. [PubMed: 3770787]

Reato D, Rahman A, Bikson M, Parra LC. Low-intensity electrical stimulation affects network dynamics by modulating population rate and spike timing. J. Neurosci. 2010; 30:15067–15079. [PubMed: 21068312]

Ren C, Tarjan PP, Popovic DB. A novel electric design for electromagnetic stimulation-the Slinky coil. IEEE Trans. Biomed. Eng. 1995; 42:918–925. [PubMed: 7558066]

Rossini PM, Marciani MG, Caramia M, Roma V, Zarola F. Nervous propagation along ‘central’ motor pathways in intact man: characteristics of motor responses to ‘bifocal’ and ‘unifocal’ spine and scalp non-invasive stimulation. Electroencephalogr. Clin. Neurophysiol. 1985; 61:272–286. [PubMed: 2411506]

Roth BJ, Cohen LG, Hallett M. The electric field induced during magnetic stimulation. Electroencephalogr. Clin. Neurophysiol. Suppl. 1991; 43:268–278.

Roth Y, Zangen A, Hallett M. A coil design for transcranial magnetic stimulation of deep brain regions. J. Clin. Neurophysiol. 2002; 19:361–370. [PubMed: 12436090]

Rothwell JC, Thompson PD, Day BL, Boyd S, Marsden CD. Stimulation of the human motor cortex through the scalp. Exp. Physiol. 1991; 76:159–200. [PubMed: 2059424]

Ruohonen J, Ilmoniemi RJ. Focusing and targeting of magnetic brain stimulation using multiple coils. Med. Biol. Eng. Comput. 1998; 36:297–301. [PubMed: 9747568]

Sadleir RJ, Vannorsdall TD, Schretlen DJ, Gordon B. Transcranial direct current stimulation (tDCS) in a realistic head model. Neuroimage. 2010; 51:1310–1318. [PubMed: 20350607]

Saypol JM, Roth BJ, Cohen LG, Hallett M. A theoretical comparison of electric and magnetic stimulation of the brain. Ann. Biomed. Eng. 1991; 19:317–328. [PubMed: 1928873]

Stecker MM. Transcranial electric stimulation of motor pathways: a theoretical analysis. Comput Biol. Med. 2005; 35:133–155. [PubMed: 15567183]

Terney D, Chaieb L, Moliadze V, Antal A, Paulus W. Increasing human brain excitability by transcranial high-frequency random noise stimulation. J. Neurosci. 2008; 28:14147–14155. [PubMed: 19109497]

Thielscher A, Kammer T. Linking physics with physiology in TMS: a sphere field model to determine the cortical stimulation site in TMS. Neuroimage. 2002; 17:1117–1130. [PubMed: 12414254]

Wagner T, Fregni F, Fecteau S, Grodzinsky A, Zahn M, Pascual-Leone A. Transcranial direct current stimulation: a computer-based human model study. Neuroimage. 2007; 35:1113–1124. [PubMed: 17337213]

Yousry TA, Schmid UD, Alkadhi H, Schmidt D, Peraud A, Buettner A, Winkler P. Localization of the motor hand area to a knob on the precentral gyrus. A new landmark Brain. 1997; 120(Pt 1):141–157.

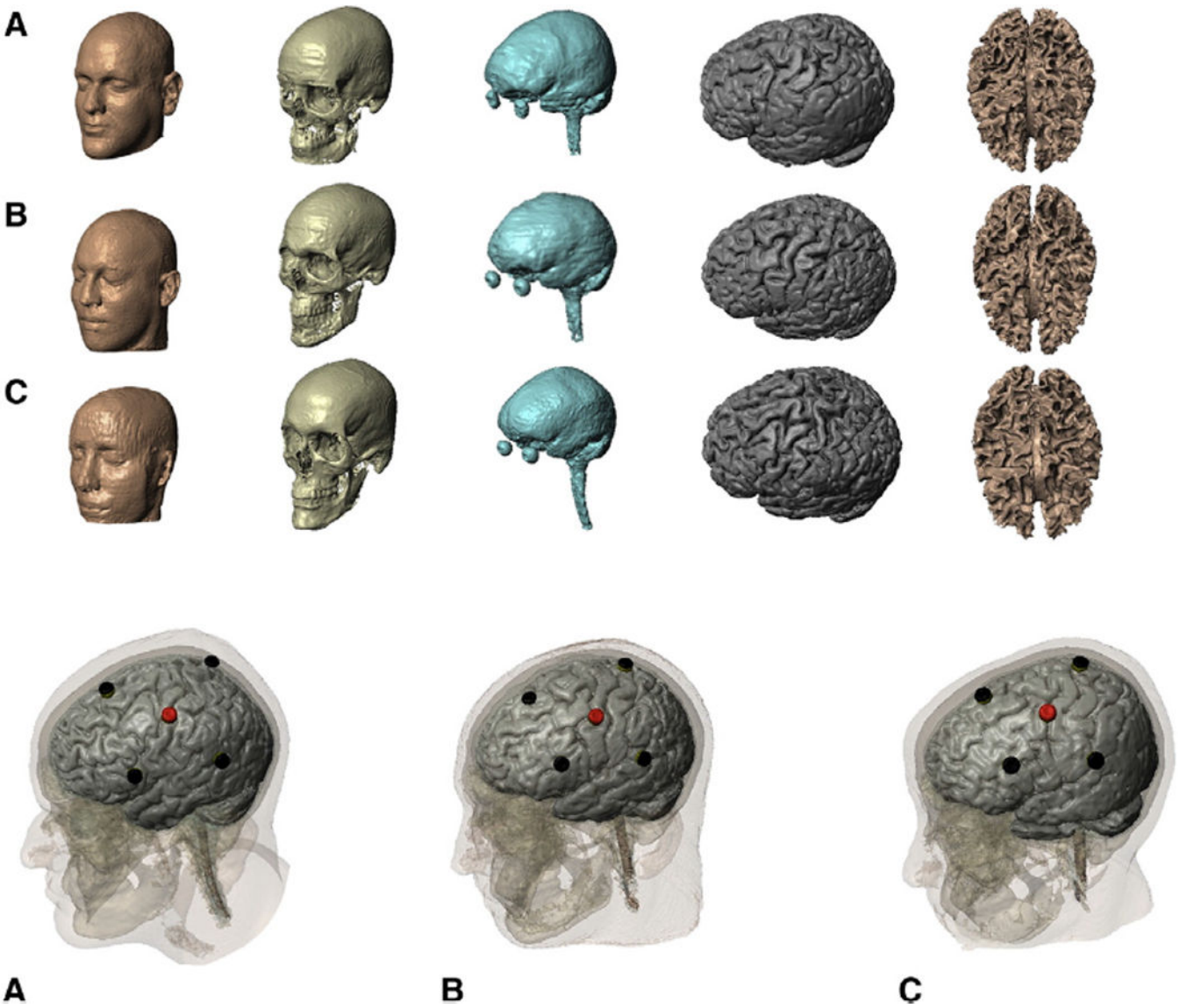

Fig. 1.

High-resolution computational models individualized from anatomical MRI. Top: The entire modeling work-flow preserved the resolution of the MRI scans (1 mm). Skin, skull, CSF, gray, and white matter masks for each individual (2 males, ages 33–40 years; see Methods). Bottom: The scalp electrode position is displayed relative to the underlying tissues for each subject (anode C3).

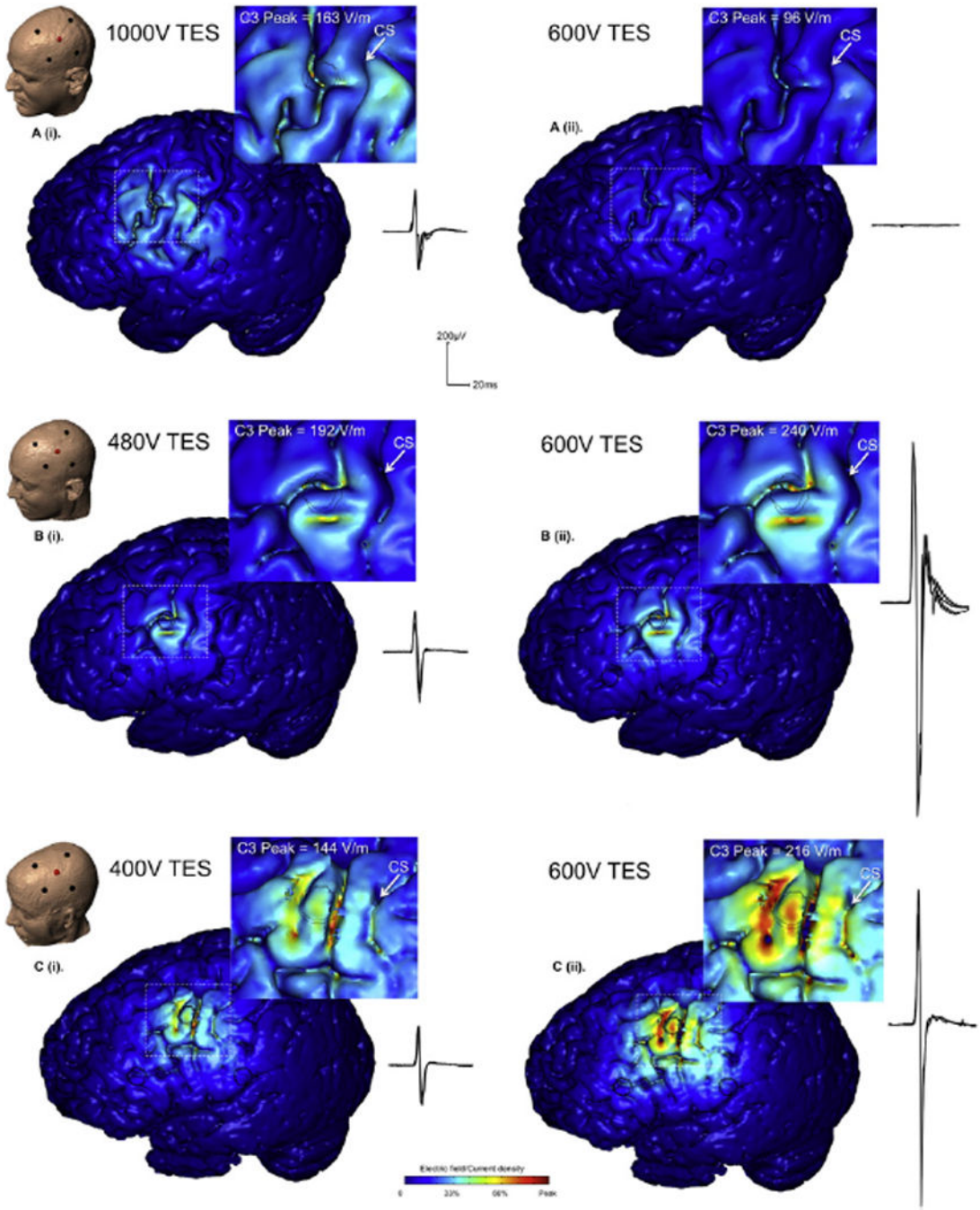

Fig. 2.

Validation of stimulation intensity: We modeled Transcranial Electrical Stimulation (TES) with a 50-μs pulse, using the High-Definition 4×1 Ring electrode montage (HD-TES), with the center 'active' electrode at position C3 (primary motor cortex hand area). Modeling data are displayed together with sample, overlaid waveforms representative of the mean amplitude recorded experimentally. The left panel; A (i), B (i), C (i) shows a range of stimulus intensities across subjects necessary to have comparable peak cortical electric field in M1. These predictions were confirmed with experimental data, where substantial input

voltage differences were required to produce comparable amplitude MEPs. The right panel; A (ii), B (ii), C (ii) shows the results from the same intensity stimulation across subjects. The model data show a vastly different amount of current delivered to the cortex across subjects. Subject A has minimal current delivery, whereas Subjects B and C have strong current delivery. The model predictions are again consistent with the experimental data showing no evoked responses in Subject A, and strong evoked responses in subjects B and C.

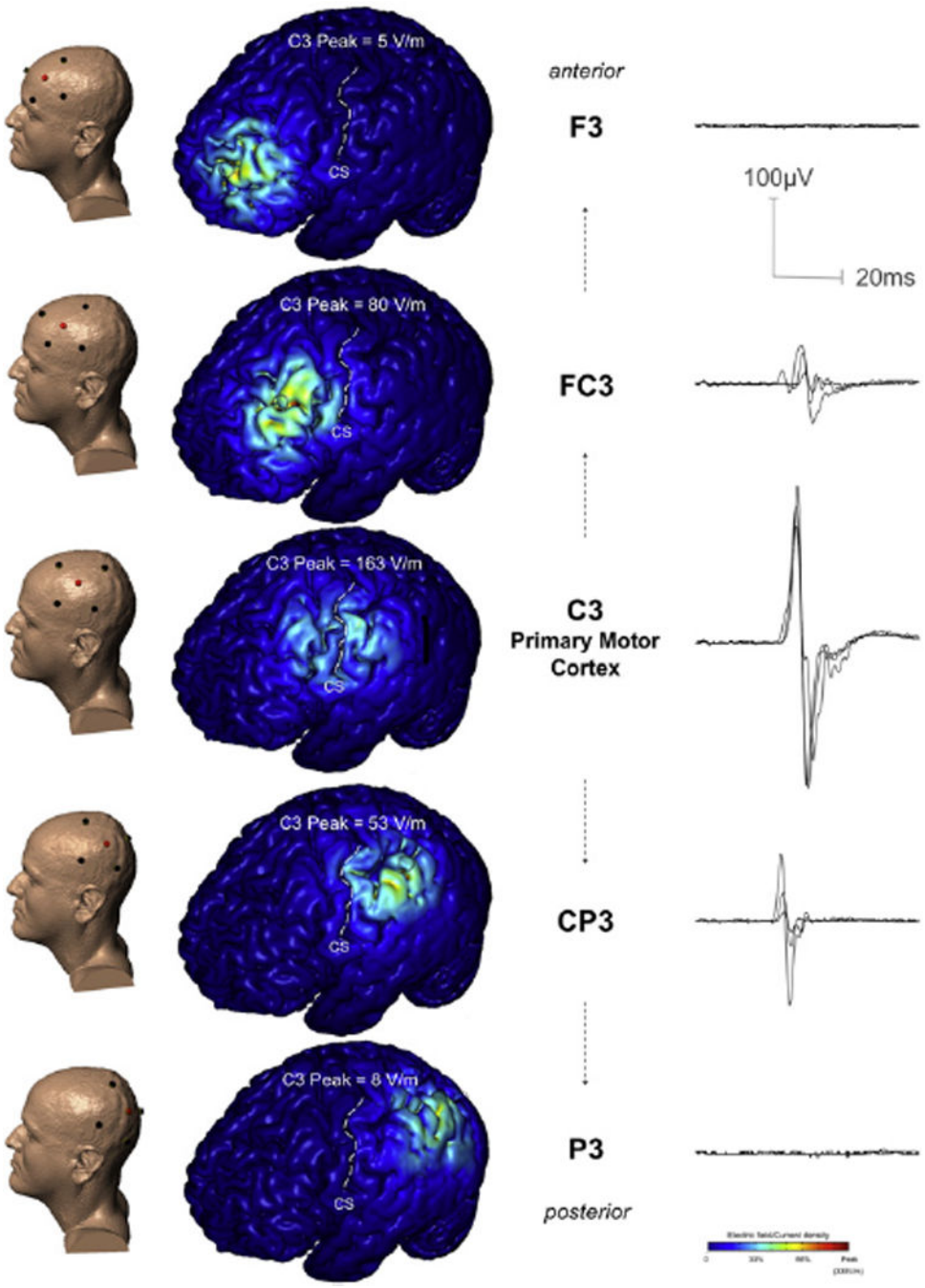

Fig. 3.

Modeling and experimental data (overlaid waveforms) from one subject (Subject A), illustrating the effect of TES at and away from C3 on predicted current density in M1 and corresponding MEPs in the hand. In addition to the C3 position, directly over primary motor cortex, the TES 4×1 montage was positioned in two anterior and two posterior positions, in each case moving away from the C3 position by approximately the distance of the circle radius (~3 cm). The four return 'ring' electrodes were also positioned using the 10/20 EEG system. Finite element analysis predicted brain current flow for each montage: the resulting

cortical electric field magnitude (false color map) are shown in each case. In all three cases, the model predicts that High-Definition TES results in significant brain stimulation (>30% of peak) restricted to inside the ring perimeter, under the active center electrode. In this way, only the C3 centered case produces significant stimulation of motor regions.

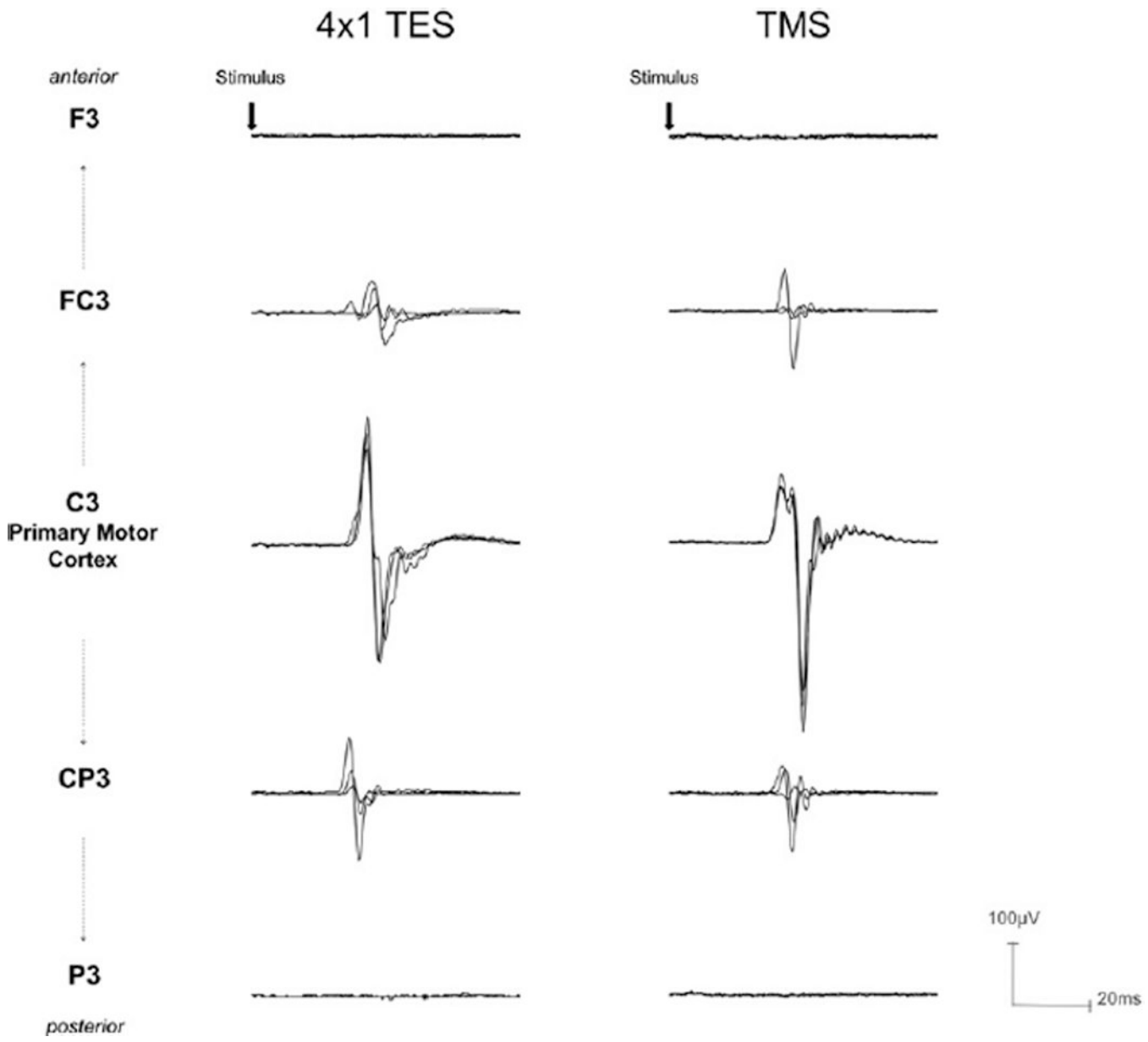

Fig. 4.

Sample overlaid MEP waveforms from Subject A in response to TES (left panel) and TMS (right panel) with intensity adjusted to elicit 0.3–0.5 mV amplitude. Consistent responses occurred with stimulation over C3, but the same intensity stimulation moved to the 1-R distance from C3 could only weakly generate MEPs, and no response could be elicited with stimulation at the 2-R positions. This effect was independent of movement in the anterior or posterior directions, and no difference in this spatial relationship could be distinguished between TES and TMS. This provides direct evidence that the 4×1 montage can deliver current to cerebral cortex without substantial current spread.

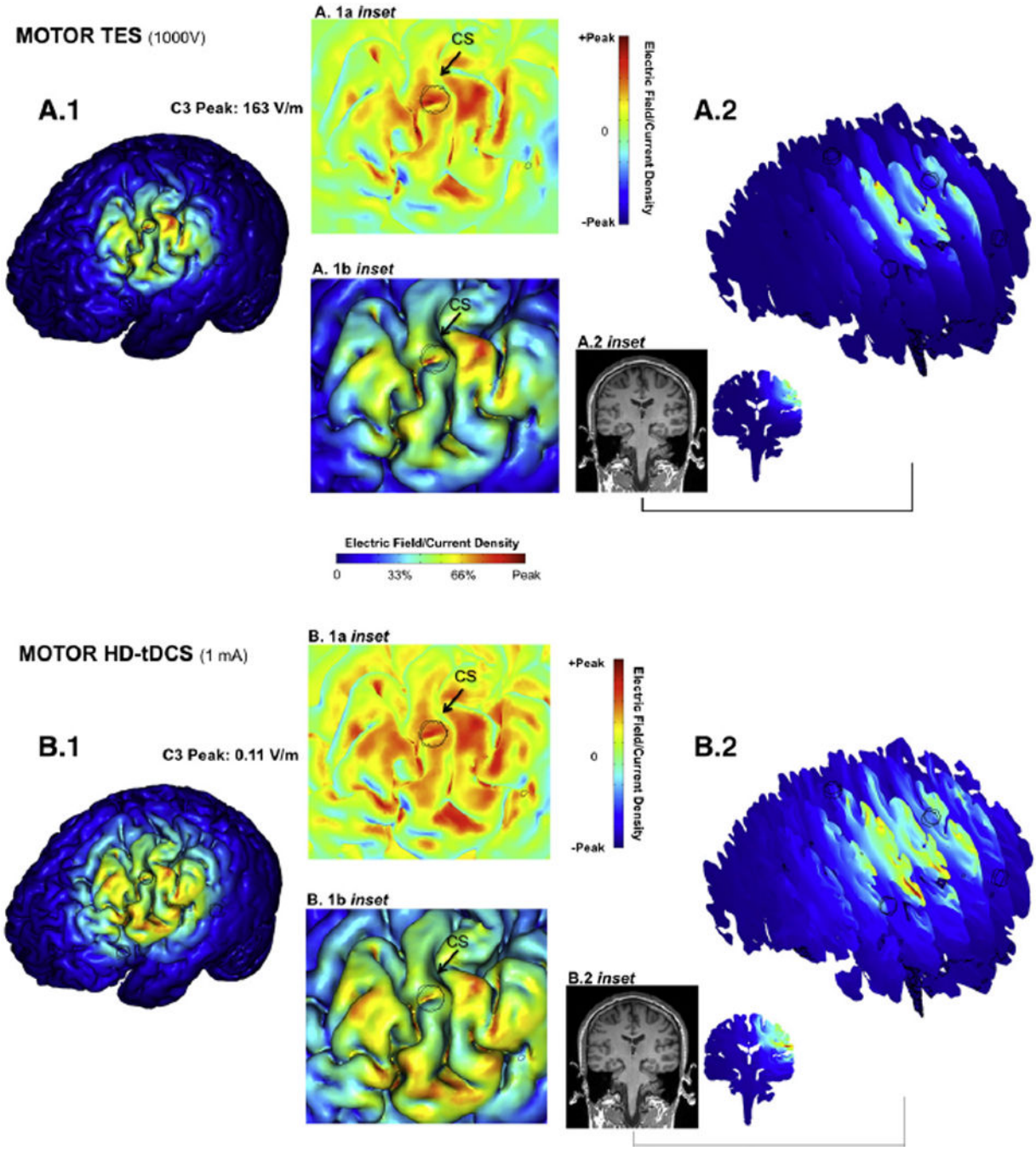

Fig. 5.

High-resolution computer simulation prediction of relative focality of Transcranial Electrical Stimulation (TES) and transcranial Direct Current Stimulation (tDCS) using the High-Definition 4×1 Ring Configuration. Using the identical High-Definition 4×1 electrode montage centered on C3, the relative brain stimulation focality using a high-voltage short-pulse (TES, *A*, same conditions as Fig. 2 plotted full scale) and low-intensity direct current (tDCS, *B*) was calculated (see Methods). In each case, the resulting cortical electric field magnitude is plotted relative to the respective peak cortical electric field induced for each

waveform: 163 V/m for TES, and 0.11 V/m for tDCS. The false-color maps thus indicate the spatial distribution of brain stimulation and relative focality in each case. For both $TES_{4\times1}$ and $tDCS_{4\times1}$: 1) The relative brain surface activation (>30% peak) was generally restricted to inside the ring (*A.1*, *B.1*) but the relative spatial distribution was slightly broader for tDCS; 2) The electric field was slightly more superficial for the $TES_{4\times1}$ waveform (*A.2*, *B.2*); 3) The peak cortical electric field (*A.1b inset*, *B.1b inset*) was on gyri crowns, interestingly in both cases on the same gyrus slightly posterior to the center electrode; 4) Consideration of normal direction current (*A.1a inset*, *B.1a inset*) red: inward; green: no normal current; blue: outward) did not change the above findings.

Table 1

Modeling and experimental data for each subject, showing the effect of stimulus location on M1 current delivery. Predicted stimulus intensity at C3 necessary for suprathreshold current density in M1, could elicit evoked responses experimentally. The same intensity delivered at the 1-R position was predicted to deliver a current density to M1 approximately in the range of motor threshold, and was confirmed experimentally, with weak responses in the 1-R positions. Model predictions for insufficient current to reach M1 in the 2-R positions also held true when tested experimentally, since no MEPs were observed at this distance. These findings were observed for each of the subjects and supports the focality of the 4×1 montage where the majority of current is confined within the electrode ring. TES was voltage controlled (see methods) with device reported current also indicated.

			TES Input at Scalp		**Cortical current density (V/m)**			**Muscle Response**	
			Voltage (V)	Current (mA)	C3 peak	M1 Range	Sagittal	MEP (mV)	
	Anterior								
		F3	1000	1817 ± 15	5	0–45	0–4	<0.00	✗
		FC3	1000	1773 ± 2	80	40–135	20–80	0.08 ± 0.03	Weak
SUBJECT A	↑ *M1* ↓	C3	1000	1738 ± 1	163	50–163	65–90	0.3 5 ± 0.07	✓
		CP3	1000	1038 ± 8	53	40–81	30–49	0.06 ± 0.03	Weak
		P3	1000	1761 ± 6	8	1–12	4–13	<0.00	✗
	Posterior								
			Voltage (V)	Current (mA)	C3 peak	M1 Range	Sagittal	MEP (mV)	
	Anterior								
		F3	550	1202 ± 3	36	19–50	25–31	<0.00	✗
		FC3	480	1019 ± 1	67	24–98	34–43	<0.00*	✗
SUBJECT B	↑ *M1* ↓	C3	480	1138 ± 0	192	29–228	72–152	0.45 ± 0.12	✓
		CP3	480	1062 ± 1	29	19–48	22–44	<0.00*	✗
		P3	600	1439 ± 1	18	36–120	12–26	<0.00	✗
	Posterior								
					* with muscle contraction 0.7 ± 0.04 mV (FC3), 0.34 ± 0.06 mV (CP3)				
			Voltage (V)	Current (mA)	C3 peak	M1 Range	Sagittal	MEP (mV)	
	Anterior								
		F3	750	933 ± 7	59	15–68	42–51	<0.00	✗
SUBJECT C	↑ *M1* ↓	FC3	400	491 ± 0	76	32–80	44–64	<0.00*	✗
		C3	400	709 ± 0	144	46–146	72–100	0.46 ± 0.08	✓

	TES Input at Scalp		Cortical current density (V/m)			Muscle Response	
Posterior	CP3	400	52	28–68	28–38	<0.00*	✗
	P3	750	29	25–30	11–26	0.01 ± 0.00	✗
		623 ± 1					
		975 ± 5					

* with 600V, 0.020 ± 0.01 mV (FC3), 0.04 ± 0.01 mV (CP3)